ACS OMEGA

http://pubs.acs.org/journal/acsodf

Article

Synthesis and Characterization of Polypyrrole Film Doped with Both Molybdate and Salicylate and Its Application in the Corrosion Protection for Low Carbon Steel

Vu Quoc Trung, Ha Manh Hung, Le Van Khoe, Le Minh Duc, Nguyen Thi Bich Viet, Duong Khanh Linh, Vu Thi Huong, Nguyen Dang Dat, Doan Thi Yen Oanh, Ngo Xuan Luong, Nguyen Thuy Chinh, Hoang Thai, Hoang Thi Tuyet Lan, Cao Long Van, Ştefan Ţălu, and Dung Nguyen Trong*

Cite This: *ACS Omega* 2022, 7, 19842−19852

Read Online

ACCESS | Metrics & More | Article Recommendations

ABSTRACT: Polypyrrole (PPy) films doped with molybdate and salicylate have been successfully electropolymerized on low carbon steel in aqueous solutions containing both molybdate and salicylate in a one-step process that did not require any pre-treatment of the steel substrate. Salicylate-doped PPy films were synthesized in the same way for comparison. The steel surface was rapidly inhibited and the PPy-based films were formed on it easily. The PPy-based films were characterized by Fourier transform infrared, scanning electron microscopy, energy dispersive X-ray, and thermal gravimetric analysis methods. The corrosion protection performance of the coatings was investigated with electrochemical impedance spectroscopy, open circuit potential (OCP), salt spray test, and Tafel polarization. It was found that in the presence of both molybdate and salicylate as dopants, the films on steel could present a better corrosion resistance than PPy film doped with only salicylate. The self-healing property of PPy-based films was observed on the OCP measurement with the fluctuation of rest potential. The salt spray test results showed that the PPy film doped with both salicylate and molybdate was more salt-resistant than the PPy film doped with only salicylate. The results suggest that the PPy coatings doped with both molybdate and salicylate are potential for application as metallic anti-corrosion coatings.

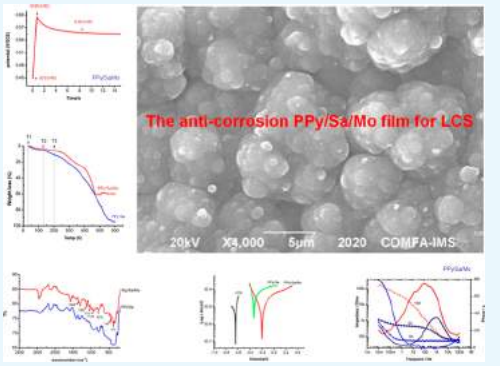

1. INTRODUCTION

Nowadays, metals, alloys in general and low carbon steel (LCS) in particular, are the most common material widely used in all areas of economic and social life. Metals such as Ni,[1,2] Fe,[3−5] Al,[6,7] and Ag;[8] alloys such as FeCoNi,[9] CuAu,[10] Fe_2O_3,[11] AgAu,[12] FeC,[13] AlNi,[14] AuCu,[15] NiCu,[16−18] and NiFe;[19,20] nonmetallic polymers;[21,22] and polymer−metals[23] have good properties such as durability, fire protection, and good electrical conductivity. When metal or nonmetallic dopants are introduced into polymers, their conductivity increases.[21−23] Their highest disadvantage is that they can oxidize or corrode when they are exposed to the environment as microbial corrosion in petroleum and industrial wastewater,[24,25] the biodegradation of hydrocarbons,[26] and the methanol extract from marine algae inhibit the corrosion ability of steel in sodium chloride medium.[27] Corrosion of metals and alloy destroy metal and alloy structures, reduce their lifetime, and consume significant amounts of metals and alloy. Thus far, protecting metals and alloys from corrosion is always a difficult and costly issue. Among a wide range of methods to prevent metal and alloy corrosion, creating coatings has always been of interest for its low cost, ease of implementation, and efficiency. To create a film, which is resistant to the corroding of the environment, there are many methods. The most used method today is the electrochemical method, which is the cheapest and the most cost effective.[28−31] In particular, the role of the electrode determines the effectiveness, quality, and applicability of the product. Electrodes include many types such as glass carbon electrodes, boron-doped diamond, graphene, carbon screen-printing electrode, and so on; they are mainly applied in pharmaceutical fields.[32−35] In the fields of science and technology, researchers also use the low carbon bare electrode,[36−38] which has been widely used due to its low cost, chemical inertness, and increasing capacity for applicability in practice. Three

Received: March 17, 2022
Accepted: May 20, 2022
Published: June 3, 2022

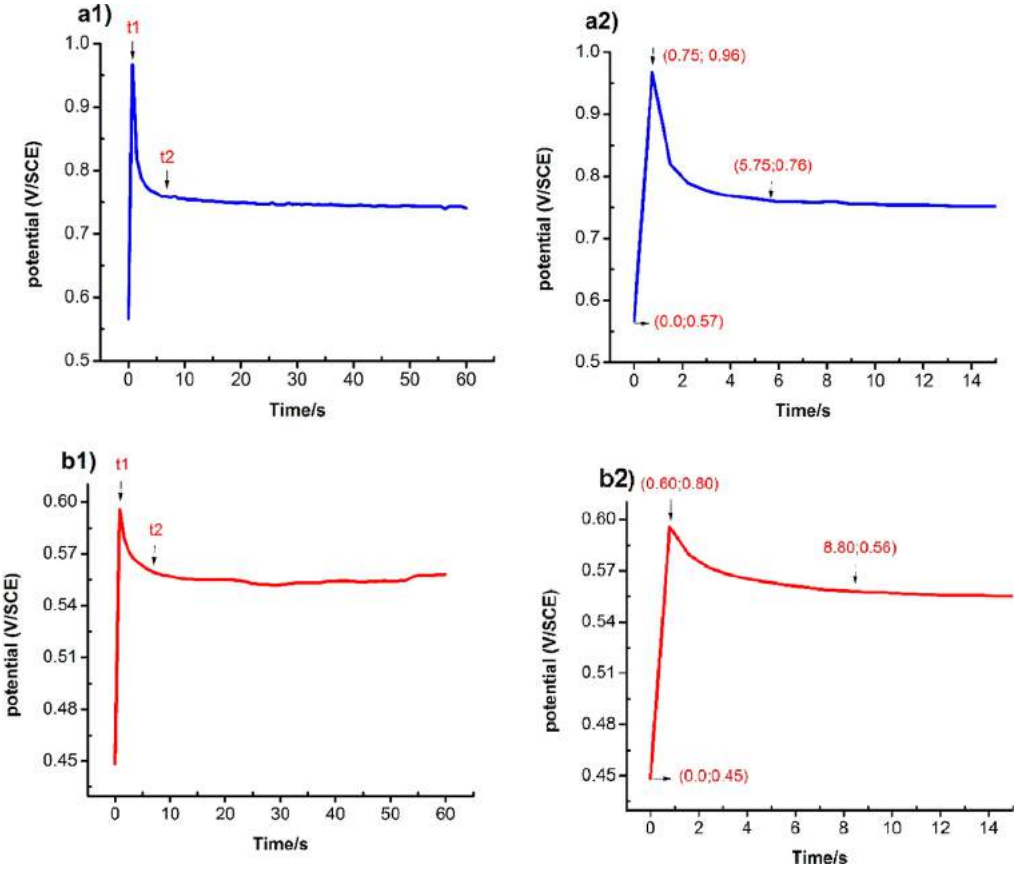

Figure 1. Potential vs time curves of electropolymerization of PPy in PPy/Sa (a1,a2) and PPy/Sa/Mo (b1,b2) solutions.

scientists—Heeger, Shirakawa, and MacDiarmid—made a breakthrough in the successful study of polymer materials capable of conducting electricity, and as a consequence, they won the prestigious Nobel Prize in Chemistry in 2000.[39] By 2003, 2021 there are successful research works on the ability to reduce corrosion in industrial wastewater, petroleum, and acid environments.[24−27] In recent research, scientists have successfully investigated the possibility of increasing the electrical conductivity of polymer materials by doping metals.[23] Scientists referred to this material as polypyrrole (PPy) material. PPy is one of the materials that have excellent properties such as high conductivity, stability, easy synthesis, and good bio-compatibility. Especially, it has better eco-friendly properties than polyaniline or polythiophene. Using PPy-based coatings for corrosion protection becomes a potential approach in the anti-corrosion of metals, which can be considered a sustainable alternative to toxic chromate-based coatings.

The aim of this study was threefold: (i) to electrochemically synthesize PPy coatings on LCS substrate by a one-step process in the solution containing both salicylate and molybdate anions; (ii) to characterize the doped PPy coatings; and (iii) to evaluate the role and synergetic effect of salicylate and molybdate dopants in corrosion protection for LCS. In our recent article,[22] we have simulated numerically the structure and band gap of some polymers (using copyrighted Material Studio software at the Center of Computational Science of Hanoi University of Education, Viet Nam); also, the numerically simulated results can be compared with experimental ones.

To explain the corrosion inhibition mechanism of PPy coatings, the mechanism of anodic passivation,[40,41] physical barrier,[42] complex formation,[43] and self-healing[44,45] have been proposed. PPy coatings provide stabilization of passive films on the metal substrate through coupling interactions;[46,47] therefore, they can enhance the corrosion inhibition in aggressive environments.[48] However, single PPy coatings exhibit some disadvantages. They may lose their protective behavior due to some small defects in the polymer layer. In the presence of defects, the barrier mechanism does not work and corrosion takes place at these defects, resulting in the peeling of the film. Consequently, the iron substrate is not protected anymore. This problem can be tackled if the dopant anions are mobile enough to be easily released from the PPy film in the oxidation-reduction reactions and moved to the corrosion site. Dopants and metal ions can then form an insoluble salt in the defects of the metal surface. The defects are thus passivated and healed. Such coatings are so-called self-healing.[49−53] Besides, although electrochemical synthesis is known to be cleaner and easier to control the coating thickness and morphologies compared to chemical polymerization, it is really difficult to electrochemically synthesize PPy films on active metal substrates such as iron because they dissolve very fast before the pyrrole (Py) monomers can reach the electrode surface. This results in poor adhesion, even the peeling of the films. Some kinds of anions can inhibit the dissolution of iron and promote the oxidation of Py monomers on active substrates. The role of dopant anions in improving corrosion protection by conductive polymers has been largely discussed.[54−62] The protective behavior of conductive polymer films can be controlled by changing different types of dopant

https://doi.org/10.1021/acsomega.2c01561
ACS Omega 2022, 7, 19842−19852

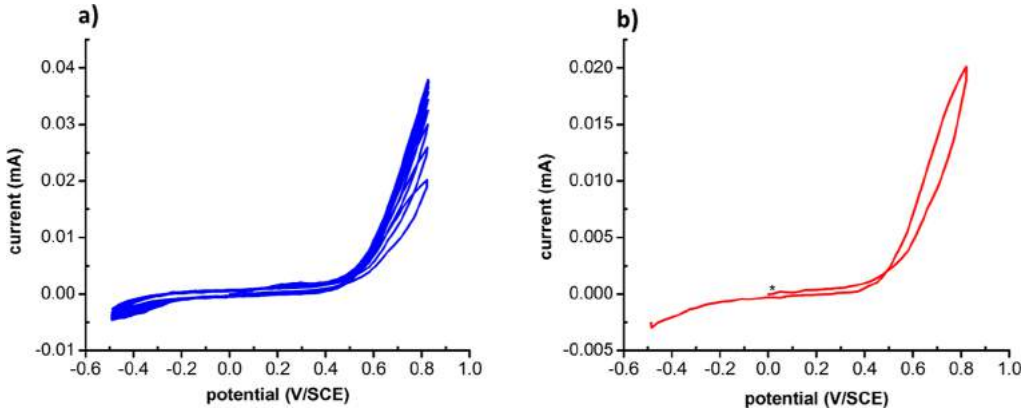

Figure 2. Cyclic voltammogram curves (a), with the first cycle (b) of electropolymerization of PPy in solution PPy/Sa/Mo.

anions that are corrosion inhibitors. Inhibition dopants can provide the barrier effect, and some dopants can introduce passivation, such as dodecyl sulfate and oxalate ions,[54] molybdate,[24,55,56] phosphate,[57] polyvinyl acetate,[58] tungstate,[59] ammonium oxalate,[60,61] phosphotungstate,[62] dodecylbenzene sulfonate, *p*-toluene sulfonate, and 2-naphthalene sulfonate composite pigments.[63] Besides, salicylate ion has been also known as an effective inhibitor dopant of PPy film on iron.[64−66] In our recent articles, it was discussed that molybdate dopant can play a role as an inhibitor for PPy smart coatings. Single doping with molybdate anion into PPy films or ion exchange by the polarization of PPy films was reported to provide a self-healing effect for PPy coatings on iron.[67−69] They can be released from the film during the reduction process and keep the open circuit potential (OCP) of iron in the passive zone for a long time. Doping both salicylate and molybdate anions into PPy films may be thus expected to enhance even more the corrosion protection performance of LCS. To our best knowledge, this approach has not been much explored. In a recent paper, we tried to electrochemically synthesize PPy coatings on an LCS substrate by a one-step process in the solution containing both salicylate and molybdate anions. Also, we characterized the doped PPy coatings and evaluated the role and synergetic effect of salicylate and molybdate dopants in corrosion protection for LCS.

2. RESULTS AND DISCUSSION

2.1. Electrochemical Polymerization. Typical potential−time curves obtained during the deposition of PPy at 1 mA/cm^2 in PPy/Sa and PPy/Sa/Mo solutions are shown in Figure 1.

It is observed that, once the current was imposed, the potential instantaneously increased due to double-layer charging effects and the nucleation process. Electrode passivation was immediate as immersion. Then, the potential starts to decrease at t_1, t_2 [Figure 1(a1)]. The process shows that from the initial time corresponding to the potential 0.57 V/SCE to the next time t_1 = 0.75 s, the potential increases linearly from 0.57 to 0.96 V/SCE. When increasing the time from t_1 = 0.75 s to t_2 = 5.75 s, the potential decreases logarithmically and reaches saturation value at 0.76 V/SCE [Figure 1(a2)]. At 5 s, the potential is stabilized at constant values corresponding to the oxidation potential of pyrrole. The obtained results show that the non-inducible polymerization leads to hindrance of the dissolution of LCS and creates a passivation layer on the metal/electrolyte surface.[70] Similarly, in the case when both salicylate and molybdate anions are present in the electrolyte solution (PPy/Sa/Mo), the results show an increase in potential when an electric current is applied [Figure 1(b1)]. At the initial time corresponding to 0.45 V/SCE potential, to the next time t_1 = 0.6 s, the potential increases linearly from 0.45 to 0.60 V/SCE. As the time increases from t_1 = 0.60 s to t_2 = 8.80 s, the potential decreases logarithmically and reaches saturation value at 0.56 V/SCE [Figure 1(b2)]. The obtained results show that with pyrrole oxidation, the corresponding potential value is +0.55 V/SCE, which is lower than the potential value in the case of normal oxidation, with a lower value than the potential value in the case of normal oxidation (+0.8 V/SCE). The results confirmed that the passivation layer on the LCS was strong enough to prevent the dissolution of the steel but did not interfere with the polymerization of the pyrrole. It is not a barrier to the development of PPy overlays. An opposite trend was obtained with a single-doped PPy film with molybdate,[71] where pyrrole oxidation was higher than normal.

The electropolymerization of PPy/Sa/Mo was investigated with the cyclic voltammetry (CV) technique. The CV method sweeps the voltage from negative to positive and vice versa in a fixed potential range; the monomer is oxidized to form a film on the electrode. The resulting film is also reduced and oxidized during the scanning process. The highlight of this method is that after the synthesis is complete, the films are investigated for redox properties. Oxidation and reduction peaks are shown. This is a property that any conductive polymer must have to make a protective film.

Figure 2a shows the consecutive CV cycles for the electropolymerization of PPy/Sa/Mo films in the PPy/Sa/Mo solution with a scan rate of 10 mV s^{-1}. For the first cycle (Figure 2b), the current was rapidly increased at a potential of about +0.55 V, and it was stabilized from +0.7 to +0.8 V (this result corresponded to the oxidation of monomer pyrrole). It was interesting to notice that oxidation of the pyrrole monomer occurred on LCS with the same behavior on the inert electrode. The passivation was so fast that we did not see the oxidation peak (dissolution) of iron. Without molybdate anion in the electrolyte solution, the dissolution peak of iron was observed at −0.25 V.[71] During the subsequent cycles, the LCS surface was already in a passive state, and PPy was formed. It took a certain time to passivate the LCS electrode. These results indicate that molybdate anion improved the properties of the passive layer on LCS, which affected the

https://doi.org/10.1021/acsomega.2c01561
ACS Omega 2022, 7, 19842−19852

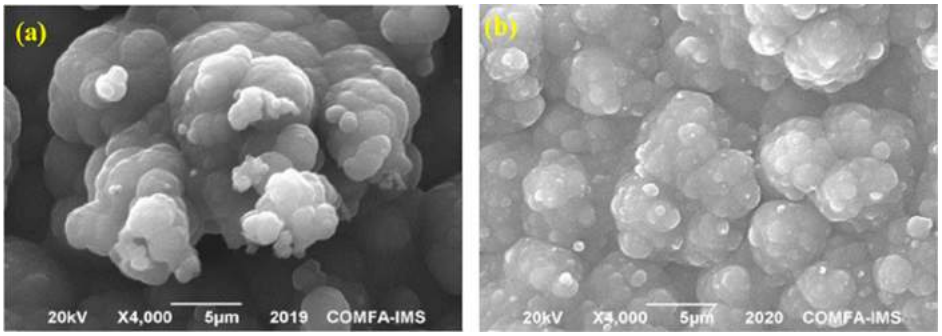

Figure 3. SEM pictures of PPy film obtained in different solutions: PPy/Sa (a); PPy/Sa/Mo (b).

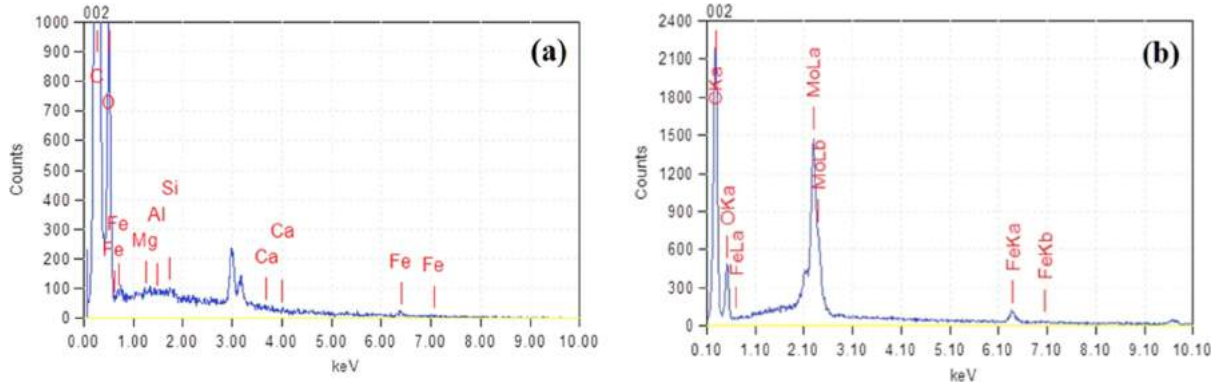

Figure 4. EDX spectra of PPy/Sa film (a); PPy/Sa/Mo film (b).

oxidation potential of the pyrrole monomer. This potential ensured the oxidation of pyrrole monomer and film formation without any difficulties on the LCS. The results obtained from the CV and potential−time curves are quite consistent.

2.2. Morphology of Doped PPy Film. The PPy films formed on LCS were quite thin, smooth, black, and homogenous. This can be seen in scanning electron microscopy (SEM) images of doped PPy films in Figure 3.

The surfaces of PPy/Sa and PPy/Sa/Mo films resulting from the PPy/Sa and PPy/Sa/Mo solutions, respectively, are characterized by a typical cauliflower-like structure of PPy coating[72,73] constituted by spherical grains (PPy balls) with different magnitudes. When doping with both salicylate and molybdate anions, the PPy/Sa/Mo film (Figure 3b) is more uniform, thinner, smoother, and more compact with smaller grains (ca. 1 μm) compared to the single-doped PPy/Sa film (Figure 3a), which exhibits a larger globular structure compared to the PPy film without dopants,[71] which shows that the role of Mo in the passivation with metal substrates is better than that of Sa. This result is consistent with other studies[71,73] and indicates that the presence of molybdate anion as a dopant in PPy films can improve the morphology of coatings on carbon steel. The successful incorporation of molybdate anion was also confirmed by energy-dispersive X-ray (EDX) analysis. Elements such as carbon, oxygen, iron, and molybdenum were detected in PPy films as shown in Figure 4.

Their percentage in the samples is given in Table 1.

It can be seen that the Mo element was doped with 17.66% to the PPy/Sa/Mo film (Figure 4b), of which Fe composition was smaller than in the PPy/Sa film (Figure 4a). It shows that when Mo is present, the amount of Fe is less dissolved than when only Sa is present. It was molybdate anion doped in the coating that inhibited the dissolution of Fe.[71]

Table 1. Element Composition in the PPy Samples

sample	C (%)	O (%)	Fe (%)	Mo (%)
PPy/Sa	75.02	21.31	3.36	0.0
PPy/Sa/Mo	56.74	23.37	2.23	17.66

2.3. Electrochemical Properties. Figure 5 shows the respective cyclic voltammograms of the PPy film obtained in monomer-free solutions with a pH of 4 by sweeping the potential from −0.8 to +1.0 V at a scan rate of 10 mV s^{-1}. It can be seen clearly from Figure 5 that anodic and cathodic peaks appeared for all cycles. The curves show that the PPy polymer can be doped and undoped electrochemically, indicating that the polymer coating remains electroactive during the potential sweepings. When the electrolyte solution contained only salicylate anion, in the first CV cycle, a pair of strong oxidation and reduction peaks appeared at about −0.2 and −0.4 V, respectively (Figure 5a). For the subsequent cycles, the anodic peak increased with the number of scan cycles, maybe due to the completion of the PPy film growth. However, after 5 scan cycles, the cycles were reversible, and the anodic peak kept steady. Meanwhile, the cathodic peak moved to the positive potential with the increase in sweeping cycles. This was associated with the release of dopants from the PPy film. It can be said that the PPy film still maintained its electrochemical properties while dopants could be incorporated into or released from the PPy film during the redox process. When the peaks of redox and reduction change a little after scan cycles, the redox process is stable. In the free-monomer solution containing both salicylate and molybdate anions, the electrochemical behaviors of the PPy film are quite different (Figure 5b). In this case, anodic and cathodic peaks were at more negative potentials compared to the previous

https://doi.org/10.1021/acsomega.2c01561
ACS Omega 2022, 7, 19842−19852

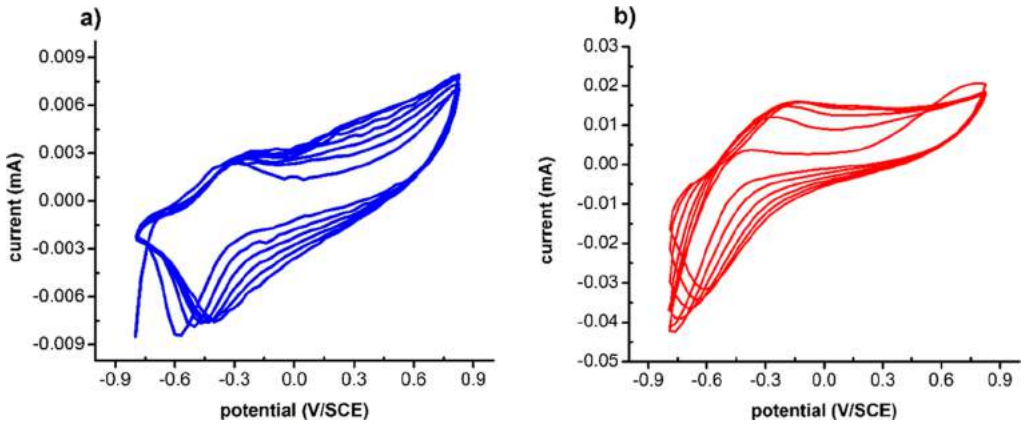

Figure 5. CV curves of the PPy film on LCS in monomer-free solutions: 0.1 M salicylate (a) and 0.1 M salicylate + 0.01 M molybdate (b) with a scan rate of 10 mV s^{-1}.

ones in the salicylate solution. This resulted from the doping of both molybdate and salicylate anions into the PPy film, which shifted the redox peaks. The doping or releasing of both dopants into/from the polymer film could affect the redox behavior of PPy because it was reported that the size and mobility of dopants had some effects on the redox behavior of the PPy film.[49,53] In this case, it seems that the molybdate dopant was incorporated into or released from the PPy film at the same time as the salicylate dopant. This led to the change in redox peaks of PPy.

2.4. FTIR Study. The Fourier transform infrared (FTIR) spectra of PPy/Sa and PPy/Sa/Mo films were investigated in the wavelength range from 600 to 2800 cm^{-1}; the corresponding results are shown in Figure 6.

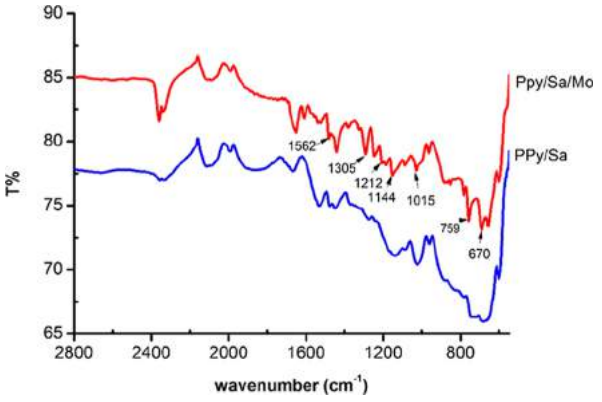

Figure 6. FTIR spectra of the Ppy/Sa/Mo film.

Absorption bands at 670, 872, and 1015 cm^{-1} were attributed to the out-of-plane and in-plane C−H bending vibration of the aromatic rings. The peaks at 1144, 1212, 1562, and 2672 cm^{-1} could be assigned to the vibration of the pyrrole ring and stretching vibrations of C−C, C═C, and ═C−H in salicylate and pyrrole structures. The band at 1667 cm^{-1} was characteristic of the stretching of salicylate C═O (Figure 6). The bending vibration of the N−H bond in PPy and O−H bond in salicylate appeared in the range of 1449−1529 cm^{-1}, whereas the peaks at 759 and 1305 cm^{-1} were the stretching vibrations of MoO_4^{2-}.[71] The FTIR results indicate that the PPy films were successfully synthesized with the incorporation of salicylate dopant or both salicylate and molybdate.

2.5. TGA Characterization. Figure 7 shows the thermal gravimetric analysis (TGA) curves of PPy/Sa (dark blue) and

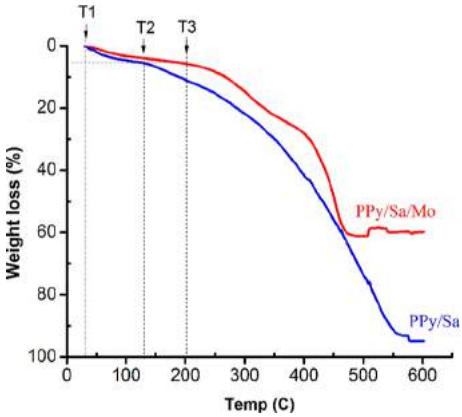

Figure 7. TGA curve of PPy/Sa film and PPy/Sa/Mo film.

PPy/Sa/Mo (red) samples, which allow us to analyze their thermal stability. The first weight loss of PPy/Sa (50−150 °C) and PPy/Sa/Mo (50−200 °C) was assigned to the evaporation of water inside the polymer samples. The second one (200−450 °C) could be due to the decomposition of dopants and residue monomers. The third stage (450−600 °C) was the breaking down of the C chains and thermal degradation of the polymer. At the end of the analysis (600 °C), there was 40% (w/w) residue of PPy/Sa/Mo film while only 5.1% residue of PPy/Sa film. This suggests that molybdate doping could exhibit an improvement of the thermal stability of PPy film that resulted in a degradation of the PPy backbone at higher temperatures.

3.6. Corrosion Study. The corrosion performance of the doped-PPy films coated on LCS was investigated using OCP curves.

Figure 8 shows the OCP curves of the doped PPy samples after immersion in 3% aerated NaCl solution. In the first stage of immersion, both samples remained OCP at relative positive potentials. OCP is the corrosion potential; if this is more positive, it means that the metal will fall into a passive state, leading to inhibited corrosion and enhanced protection of the metal. Over time, Cl^- in the solution (corrosion agent) passes through the membrane, contacts the metal substrate, and corrosion occurs; at this time, the metal is corroded, and the

https://doi.org/10.1021/acsomega.2c01561
ACS Omega 2022, 7, 19842−19852

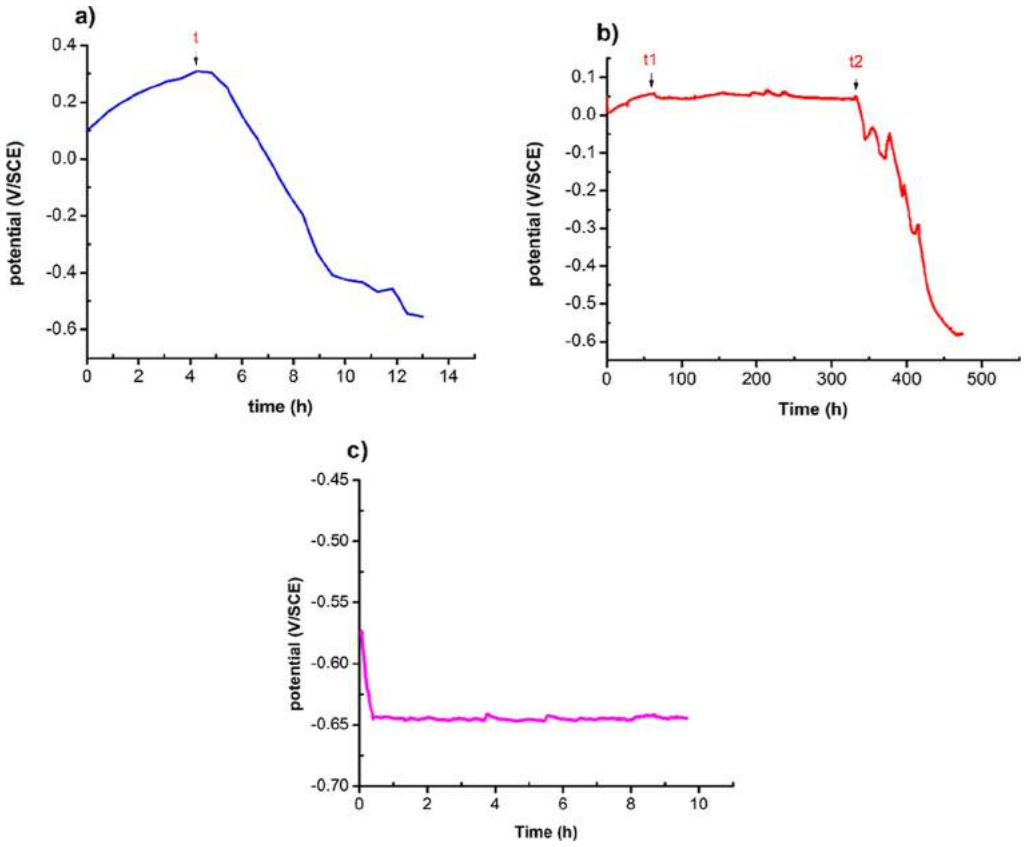

Figure 8. OCP of PPy/Sa film (a) and PPy/Sa/Mo film (b); LCS (c) samples in 3% aerated NaCl solution.

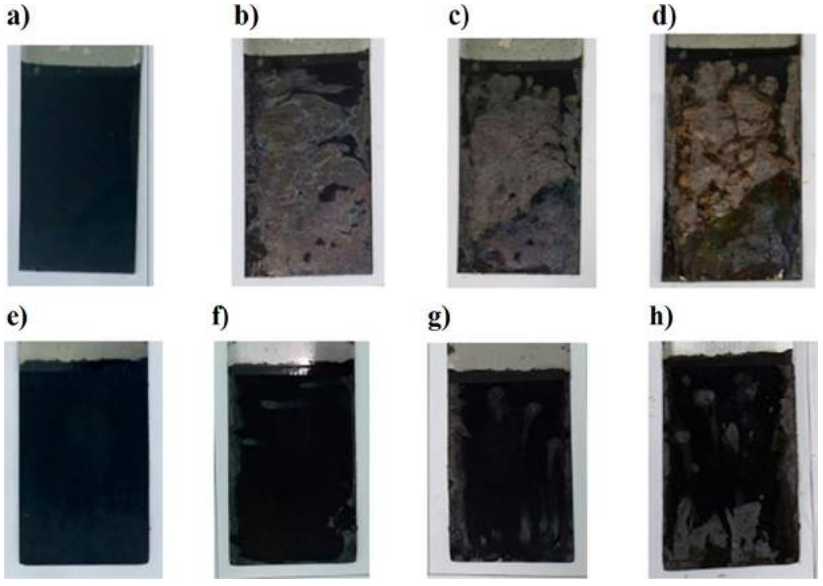

Figure 9. Photographs of PPy/Sa film (a–d) and PPy/Sa/Mo film (e–h) on LCS after exposure to salt spray for 0 (a,e); 3 (b,f); 9 (c,g); 21 h (d,h).

potential changes to a negative value. When observing the change in OCP, it will be possible to judge whether the base metal has been corroded or not. If the value of OCP is close to the corrosion potential value, it can be concluded that metal corrosion is taking place; the film is not protected as the corrosion potential of Fe is (−0.55 V) [compared to saturated calomel electrode (SCE)]; if OCP measured is close to this, the Fe metal will corrode. This potential stage was 5 and 350 h for PPy/Sa (Figure 8a) and PPy/Sa/Mo (Figure 8b) films, respectively. It is clear that both doped PPy films provided corrosion protection for LCS substrates. The substrates were in a passive state and well protected. A slight increase in OCP in this region can be observed. It may present the anion exchange of salicylate and molybdate dopants with chloride anions in the electrolyte. Then, a slight decrease can be seen in both samples. Interestingly, slight fluctuations of potential can

https://doi.org/10.1021/acsomega.2c01561
ACS Omega 2022, 7, 19842−19852

be observed in the PPy/Sa/Mo sample in this plateau. Meanwhile, the OCP of PPy/Sa decreased gradually without any oscillations. This fluctuation of OCP in corrosion protection can be known as a self-healing mechanism. The pinholes on the coating could be passivated and activated continuously. Molybdate has been well known as the inhibitor dopant and could self-heal the film.[49,53]

In the case of PPy coating without molybdate dopant (PPy/Sa), its OCP had the same behavior as PPy/Sa/Mo coating, but the potential plateau was so short, only 5 h. After 5 h, the OCP decreased gradually and reached the corrosion potential of the bare steel. At that time, the PPy coating could not protect the steel substrate anymore. It is remarked that the fluctuation of potential was not observed. After a certain time, OCP fell to the corrosion potential of carbon steel. The PPy film could not provide further corrosion protection of LCS. It can be concluded from the OCP results that the PPy film doped with molybdate and salicylate can protect LCS from corrosion according to a self-healing mechanism.

Figure 9 shows the images of PPy samples after a certain time of exposure to the salt spray test. The salt spray method is a qualitative method used to evaluate the protective ability of a film. Based on the results obtained, determining its ability to stick, peel the outside image of the film, and compare it with other films to comment on its ability to protect. Visual observation of the PPy/Sa and PPy/Sa/Mo samples reveals that the PPy/Sa coating was damaged from 0 to 3, 9, and 21 h of exposure (Figure 9a–d), whereas the PPy/Sa/Mo coating samples still adhered to the LCS.

Although there were still some blisters and damage points on the PPy/Sa/Mo coating, brown rust could not be observed on it (Figure 9e–h). The PPy/Sa coating was almost peeled off and an iron oxide layer was formed (Figure 9d). The process of salt spray and photography was done by the members of the author group, Nguyen Thuy Chinh and Hoang Thai, at the Institute for Tropical Technology, Vietnam Academy of Science and Technology.

Molybdate dopant may play an important role in the inhibition of corrosion protection. It protects iron in a large area exposed to the NaCl atmosphere. The adhesion to the metal substrate of the PPy/Sa/Mo film was promoted, which resulted in an improvement of its corrosion resistance. The corrosion current and potential of the PPy/Sa and PPy/Sa/Mo coatings and bare LCS were also recorded in a 3% NaCl solution (Figure 10).

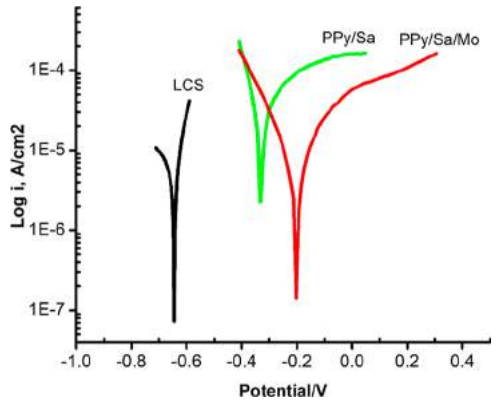

Figure 10. Tafel plot of LCS, PPy/Sa film, and PPy/Sa/Mo film in 3% NaCl solution.

It is obvious from the Tafel curves that lower corrosion current and higher corrosion potential have been recorded for the Ppy/Sa/Mo (red) coating. Tafel is a tool used to measure corrosion currents represented by current–potential graphs and extrapolate two branches, anode and cathode. Then, the point of intersection is the corrosion current and potential. Here, the corrosion current is shown in the presence of molybdate doping substances; if the corrosion current is small, it shows that they are less corroded. The corrosion potential E_{corr} of the PPy/Sa/Mo film shifted toward positive values compared to that of PPy/Sa (blue) film and LCS (black). Also, the corrosion current was smaller than that of PPy/Sa film and LCS.

The calculated anti-corrosion currents were used to know the corrosion inhibition efficiency (η) of Ppy/Sa and Ppy/Sa/Mo with LCS, according to eq 1

$$\eta = \frac{I_{corr}^{0} - I_{corr}}{I_{corr}^{0}} \times 100\% \quad (1)$$

where I_{corr}^{0} and I_{corr} are corrosion currents of bare LCS and Ppy-coated LCS, respectively. The anti-corrosion efficiency of the Ppy/Mo/Sa sample is 92.6% and that of Ppy/Sa is 53.8%, which shows that the anti-corrosion performance of Ppy/Sa/Mo is larger than that of Ppy/Sa.

From the extrapolation of Tafel curves, the corrosion current density (I_{corr}) and corrosion potential (E_{corr}) of the PPy/Sa and PPy/Sa/Mo samples were 3.7×10^{-5}, 5.9×10^{-6} A cm^{-2}, respectively (Figure 10). The I_{corr} values of PPy/Sa/Mo sharply decreased in the presence of molybdate in the coating.

It is indicated that the incorporation of molybdate anions significantly enhanced the corrosion resistance. Molybdate dopant helped to form a more resistive PPy coating. The results obtained from this corrosion stream are in complete agreement with the results obtained previously. The complex compound should cover and stop the corrosion reaction at the active site. In addition, the passive film could be strengthened by the iron salicylate salt. This effect led to the enhancement of corrosion protection of PPy coating.

To understand the behavior of the coating during protection time, electrochemical impedance spectroscopy (EIS) spectra of PPy films with different dopants were recorded in 3% NaCl and are shown in Figure 11.

Figure 11 presents the Bode plots of these coatings after 5 and 10 h of immersion in a 0.1 M NaCl solution. In the presence of molybdate in PPy film, the impedance of the PPy/Sa/Mo (Figure 11b) film was higher than that of PPy/Sa (Figure 11a) and increased after 5 h of immersion. The polymer film resistance (R_{pol}) could be 10 kΩ after 10 h of immersion (Figure 9b), whereas the polymer resistance of PPy/Sa decreased after 5 h of immersion (Figure 9a). The resistance of PPy/Sa was still smaller. Bode plot of the PPy/Sa/Mo sample shows that the magnitude of the impedance increases with immersion time, which indicated the stability and good anti-corrosion properties of the coating in an aggressive solution. Here, Bode represents the change of impedance. The greater the impedance, the greater the ability of the film to protect the base metal. Because the pyrrole conducts electricity, the membrane couples with the metal base, forming an electrochemical cell. When corrosion occurs (due to the process of soaking the sample, Cl^- in the solution diffuses through the membrane, moving to the Fe surface), Fe

https://doi.org/10.1021/acsomega.2c01561
ACS Omega 2022, 7, 19842–19852

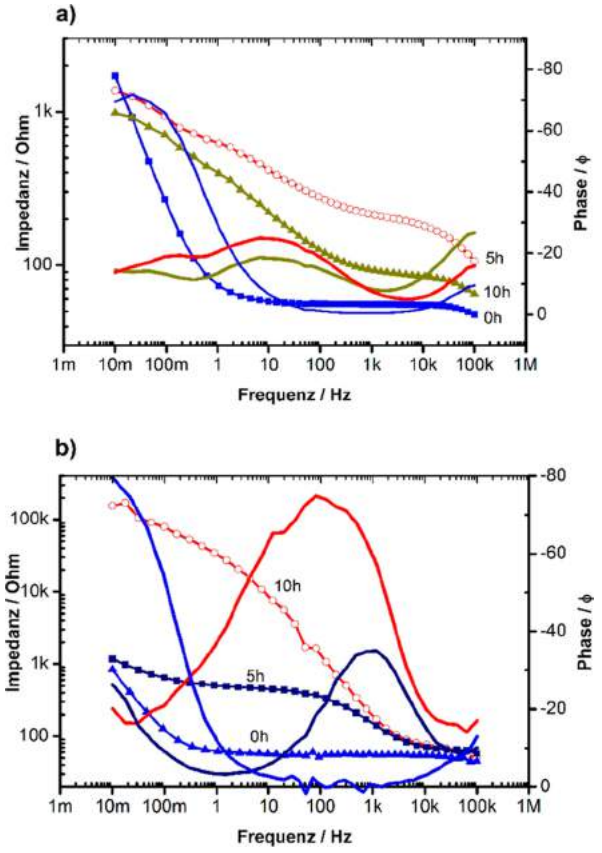

Figure 11. EIS spectra of PPy/Sa film (a) and PPy/Sa/Mo (b) film after 5 and 10 h of immersion in 3% NaCl solution.

undergoes oxidation, and the film is reduced. The reduced Ppy becomes gradually increased, inhibiting the corrosion of Fe.

3. EXPERIMENTAL SECTION

3.1. Substrate Pretreatment. Initially, we used LCS bars according to 2001-TCVN 1656-75 standard, product label TISCO Com., Thai Nguyen, Viet Nam, and the corresponding ingredient content: 0.010% P, 0.62% Mn, 0.042% S, 0.15% Si, and 0.16% C; the size of each the bar is 100 mm × 40 mm × 1 mm. To increase the smoothness of the surface of the material, they are mechanically polished with SiC papers of different roughness such as 1500, 1200, 1000, 800, and 600. Then, materials are cleaned using acetone, washed with purified water, and finally dried at room temperature, T = 300 K.

3.2. Chemicals. All chemicals such as pyrrole monomer (Py), sodium molybdate (Na_2MoO_4), and sodium salicylate were purchased from Sigma Aldrich with high purity. To do this, Py monomers were distilled before each use to remove all oligomer components and oxidized substances from the material. The oligomer is a compound formed by the self-polymerization of pyrrole monomers. Distillation is required to separate them all, to avoid being mechanically attracted to the PPy film during formation on the electrode, contaminating the PPy film. Then, the rod was placed in the dark at T = 277 K with the electrolyte solution with distilled water and previously prepared ingredients.

3.3. PPy Electrolysis on Low Carbon Materials. PPy thin films were formed at room temperature T = 300 K by electrostatic and CV measurement techniques of the Zahner workstation (Germany). CV is a widely used method in the electrochemical synthesis of conductive polymers. To electrolyze a solution containing 0.1 M pyrrole (PPy/Sa) sodium salicylate and 0.1 M sodium salicylate + 0.03 M sodium salicylate solution, Na_2MoO_4 + 0.1 M pyrrole (PPy/Sa/Mo) was prepared. Before performing the electrolysis of the material, all previous solutions were purged through nitrogen gas (N_2) to remove all oxygen from the solution. CV technique was carried out by scanning voltage from −500 to +800 mV with a scanning speed of 20 mV s^{-1} in 6 scanning cycles. After electrolysis, the resulting PPy film was washed with distilled water several times with a stream of N_2 gas and finally dried at T = 333 K after 5 h. The final result obtained was that the PPy film doped in PPy/Sa and PPy/Sa/Mo solutions was denoted as PPy/Sa and PPy/Sa/Mo, respectively.

3.4. Characterization. To study the structure of the materials, we used SEM and field emission SEM equipment of Hitachi-4800.

The infrared spectroscopy results are FTIR functions of the doped PPy films and were recorded using a Shimadzu Prestige-21 FTIR instrument set at room temperature T = 300 K with a resolution of 4 cm^{-1}, with a wave count of 400−4000 cm^{-1}.

TGA of the samples was performed on a Shimadzu TGA-50H thermal gravimetric analyzer from room temperature T = 300 K to T = 600 K with a scan rate of 283 K min^{-1} under atmospheric conditions.

SEM was used to determine the morphological characteristics of materials, FTIR was used to determine functional groups in materials, and TGA was used to investigate the change of sample mass with temperature to determine the relationship between the mass of the sample and the temperature.

3.5. Corrosion Protection Test. To measure the electrochemical impedance of the materials, we used an EIS device (German Zahner workstation) over the frequency range from 100 kHz to 10 MHz in 0.1 M NaCl solution at room temperature T = 300 K with 10 mV amplitude. For the case of Tafel polarization, electrodynamic polarization curves were obtained using a scan rate of 1 mV/s with magnetic electrode potentials between −400 and 600 mV. All the electrochemical measurements of the material were done by us on a three-electrode cell, where the counter electrode is made of a platinum plate, SCE is made of electricity reference, and working electrodes are made of LCS pads. EIS is the method used to evaluate the corrosion resistance of membranes. It is known that the working principle is based on applying a shock to a conductive system in an electrochemical system; then, the meter emits a frequency range, and the impedance of the system and the phase difference coefficient of $i(t)$ and $u(t)$ are recorded. The results obtained are the variations of R and θ. To evaluate the protective ability of the membrane, people rely on the value of R; the higher the R, the better the protection.

4. CONCLUSIONS

The PPy film doped with molybdate and salicylate was successfully electropolymerized in the electrolyte containing both dopants by a one-step process. The PPy film was smoother and denser than that of PPy film without molybdate. The film adhesion was quite good. The results show that with the use of Sa, Sa/Mo doping has improved and the ability to protect against corrosion of the film compared to LCS has increased. This is the prospect of the application of pyrrole film in anti-corrosion.

https://doi.org/10.1021/acsomega.2c01561
ACS Omega 2022, 7, 19842−19852

A reversible redox process of PPy film was observed. Molybdate can be doped into or dedoped from the PPy polymer during potential sweeping, even with the presence of salicylate dopant. The peak of oxidation and reduction was observed. Molybdate dopants were mobile enough to be released from the polymer and moved to the corrosion site.

The results showed that other properties of PPy film were also improved with molybdate doping such as morphology and thermal stability. Especially, the PPy/Sa/Mo coatings could protect LCS from corrosion with both passive film on the metal surface and the barrier effect of the coating. The corrosion test results indicated that the PPy/Sa/Mo coatings provided good protection for LCS from corrosion. OCP, EIS, Tafel polarization, and salt spray test results were the evidence to prove the enhancement of corrosion protection ability of PPy/Sa/Mo. Thus, in the presence of both molybdate and salicylate as dopants, the films on steel could present a better corrosion resistance than the PPy film doped with only salicylate. Furthermore, the PPy film doped with both salicylate and molybdate was more salt-resistant than the PPy film doped with only salicylate with an anti-corrosion efficiency of PPy/Sa/Mo of 92.6% and PPy/Sa of 53.8%. As has been mentioned in the Introduction, one can conclude that the PPy coatings doped with both molybdate and salicylate are potentially suitable for application as metallic anti-corrosion coatings.

As has also been emphasized in the Introduction, we will try to simulate numerical problems considered in this paper. This will be the subject of future publication.

AUTHOR INFORMATION

Corresponding Author

Dung Nguyen Trong − *Institute of Physics, University of Zielona Góra, Zielona Góra 65-516, Poland; Faculty of Physics, Hanoi National University of Education, Ha Noi 100000, Vietnam;* orcid.org/0000-0002-7706-1392; Email: dungntdt2018@gmail.com

Authors

Vu Quoc Trung − *Faculty of Chemistry, Hanoi National University of Education, Hanoi 100000, Vietnam*

Ha Manh Hung − *Faculty of General Education, Hanoi University of Mining and Geology, Hanoi 100000, Vietnam*

Le Van Khoe − *Faculty of Natural Sciences, Hong Duc University, Thanh Hoa City 100000, Vietnam*

Le Minh Duc − *Branch of National Institute of Occupational Safety and Health & Environmental Protection in Central of Vietnam, Da Nang 540000, Vietnam*

Nguyen Thi Bich Viet − *Faculty of Chemistry, Hanoi National University of Education, Hanoi 100000, Vietnam*

Duong Khanh Linh − *Faculty of Chemistry, Hanoi National University of Education, Hanoi 100000, Vietnam*

Vu Thi Huong − *Faculty of Chemistry, Hanoi National University of Education, Hanoi 100000, Vietnam*

Nguyen Dang Dat − *Faculty of Chemistry, Hanoi National University of Education, Hanoi 100000, Vietnam*

Doan Thi Yen Oanh − *Publishing House for Science and Technology, Vietnam Academy of Science and Technology, Hanoi 100000, Vietnam*

Ngo Xuan Luong − *Faculty of Natural Sciences, Hong Duc University, Thanh Hoa City 100000, Vietnam*

Nguyen Thuy Chinh − *Institute for Tropical Technology and Graduate University of Science and Technology, Vietnam Academy of Science and Technology, Hanoi 100000, Vietnam*

Hoang Thai − *Institute for Tropical Technology and Graduate University of Science and Technology, Vietnam Academy of Science and Technology, Hanoi 100000, Vietnam*

Hoang Thi Tuyet Lan − *Faculty of Basic Sciences, University of Transport and Communications, Hanoi 100000, Vietnam*

Cao Long Van − *Institute of Physics, University of Zielona Góra, Zielona Góra 65-516, Poland*

Ştefan Ţălu − *The Directorate of Research, Development and Innovation Management (DMCDI), Technical University of Cluj-Napoca, Cluj-Napoca 400020, Romania;* orcid.org/0000-0003-1311-7657

Complete contact information is available at: https://pubs.acs.org/10.1021/acsomega.2c01561

Author Contributions

Conceptualization: V.Q.T., L.M.D, H.T., D.N.T. Sample preparation: H.M.H., L.V.K., N.T.B.V., D.K.L., H.T.T.L. SEM, FTIR, EDX measurements: L.V.K., N.D.D., D.T.Y.O., V.T.H. Electrochemical tests: L.V.K., H.M.H., V.T.H. Salt Spray and photography: N.T.C., H.T. Data analysis: N.X.L., L.M.D. Writing—original draft: C.L.V., D.N.T., S.T., V.Q.T., L.M.D. Writing—review and editing: D.N.T., S.T., V.Q.T., C.L.V., H.T.

Funding

This research was funded by the Viet Nam National Foundation for Science and Technology Development (NAFOSTED) under grant number 104.02-2019.327.

Notes

The authors declare no competing financial interest.

REFERENCES

(1) Nguyen, T. D.; Nguyen, C. C.; Tran, V. H. Molecular dynamics study of microscopic structures, phase transitions and dynamic crystallization in Ni nanoparticles. *RSC Adv.* **2017**, *7*, 25406−25413.

(2) Dang Thi Minh, H.; Coman, G.; Nguyen Quang, H.; Nguyen Trong, D. Influence of heating rate, temperature, pressure on the structure, and phase transition of amorphous Ni material: A molecular dynamics study. *Heliyon* **2020**, *6*, No. e05548.

(3) Kien, P. H.; Lan, M. T.; Dung, N. T.; Hung, P. K. Annealing study of amorphous bulk and nanoparticle iron using molecular dynamics simulation. *Int. J. Mod. Phys. B* **2014**, *28*, 1450155.

(4) Nguyen, T. D.; Nguyen, C. C.; Nguyen, T. T.; Pham, K. H. Factors on the magnetic properties of the iron nanoparticles by classical Heisenberg model. *Phys. B* **2018**, *532*, 144−148.

(5) Trong, D. N.; Long, V. C. Effects of Number of Atoms, Shell Thickness, and Temperature on the Structure of Fe Nanoparticles Amorphous by Molecular Dynamics Method. *Adv. Civ. Eng.* **2021**, *2021*, 1.

(6) Quoc, T. T.; Trong, D. N. Molecular dynamics factors affecting on the structure, phase transition of Al bulk. *Phys. B* **2019**, *570*, 116−121.

(7) Nguyen-Trong, D.; Nguyen-Tri, P. Understanding the heterogeneous kinetics of Al nanoparticles by simulations method. *J. Mol. Struct.* **2020**, *1218*, 128498.

(8) Trong, D. N.; Chinh, C. N.; Quoc, V. D.; Quoc, T. T. Study the effects of factors on the structure and phase transition of bulk Ag by molecular dynamics method. *Int. J. Comput. Mater. Sci. Surf. Eng.* **2020**, *09*, 2050016.

(9) Cao Long, V.; Saraç, U.; Baykul, M. C.; Trong, L. D.; Ţălu, Ş.; Nguyen Trong, D. Electrochemical Deposition of Fe−Co−Ni Samples with Different Co Contents and Characterization of Their Microstructural and Magnetic Properties. *Coatings* **2022**, *12*, 346.

(10) Quoc, T. T.; Long, V. C.; Ţălu, Ş.; Nguyen Trong, D. Molecular Dynamics Study on the Crystallization Process of Cubic Cu−Au Alloy. *Appl. Sci.* **2022**, *12*, 946.

https://doi.org/10.1021/acsomega.2c01561
ACS Omega 2022, 7, 19842−19852

(11) Nguyen Trong, D.; Cao Long, V.; Ţălu, Ş. The study of the influence of matrix, size, rotation angle, and magnetic field on the isothermal entropy, and Néel phase transition temperature of Fe_2O_3 nanocomposite thin films by the Monte-Carlo simulation method. *Coatings* **2021**, *11*, 1209.
(12) Cao Long, V.; Duong Quoc, V.; Nguyen Trong, D. Ab Initio Calculations on the Structural and Electronic Properties of AgAu Alloys. *ACS Omega* **2020**, *5*, 31391−31397.
(13) Hoc, N.-Q.; Viet, L.-H.; Dung, N.-T. On the Melting of Defective FCC Interstitial Alloy c −FeC under Pressure up to 100 GPa. *J. Electron. Mater.* **2020**, *49*, 910−916.
(14) Nguyen-Trong, D.; Nguyen-Tri, P. Factors affecting the structure, phase transition and crystallization process of AlNi nanoparticles. *J. Alloys Compd.* **2020**, *812*, 152133.
(15) Nguyen-Trong, D.; Nguyen-Chinh, C.; Duong-Quoc, V. Study on the Effect of Doping on Lattice Constant and Electronic Structure of Bulk AuCu by the Density Functional Theory, Journal of Multiscale. *Modelling* **2020**, *11*, 2030001.
(16) Tuan, T. Q.; Dung, N. T. Effect of heating rate, impurity concentration of Cu, atomic number, temperatures, time annealing temperature on the structure, crystallization temperature and crystallization process of $Ni_{1-x}Cu_x$ bulk; x = 0.1, 0.3, 0.5, 0.7. *Int. J. Mod. Phys. B* **2018**, *32*, 1830009.
(17) Nguyen-Trong, D.; Nguyen-Tri, P. Molecular dynamic study on factors influencing the structure, phase transition and crystallization process of $NiCu_{6912}$ nanoparticle. *Mater. Chem. Phys.* **2020**, *250*, 123075.
(18) Trong, D. N.; Long, V. C. Factors affecting the depth of the Earth's surface on the heterogeneous dynamics of $Cu_{1-x}Ni_x$ alloy, x =0.1, 0.3, 0.5, 0.7, 0.9 by Molecular Dynamics simulation method. *Mater. Today Commun.* **2021**, *29*, 102812.
(19) Trong Dung, N. Influence of impurity concentration, atomic number, temperature and tempering time on microstructure and phase transformation of $Ni_{1-x}Fe_x$ (x = 0.1, 0.3, 0.5) nanoparticles. *Mod. Phys. Lett. B* **2018**, *32*, 1850204.
(20) Nguyen-Trong, D.; Pham-Huu, K.; Nguyen-Tri, P. Simulation on the Factors Affecting the Crystallization Process of FeNi Alloy by Molecular Dynamics. *ACS Omega* **2019**, *4*, 14605−14612.
(21) Vu, Q.-T.; Tran, T.-T. -D.; Nguyen, T.-C.; Nguyen, T. V.; Nguyen, H.; Vinh, P. V.; Nguyen-Trong, D.; Dinh Duc, N.; Nguyen-Tri, P. DFT Prediction of Factors Affecting the Structural Characteristics, the Transition Temperature and the Electronic Density of Some New Conjugated Polymers. *Polymers* **2020**, *12*, 1207.
(22) Vu Quoc, T.; Do Ba, D.; Tran Thi Thuy, D.; Nguyen Ngoc, L.; Nguyen Thuy, C.; Vu Thi, H.; Khanh, L. D.; Doan Thi Yen, O.; Thai, H.; Long, V. C.; Talu, S.; Nguyen Trong, D. DFT study on some polythiophenes containing benzo[d]thiazole and benzo[d]oxazole: structure and band gap. *Des. Monomers Polym.* **2021**, *24*, 274−284.
(23) Vu Quoc, T.; Duong, L. T.; Quoc, V. D.; Tran Quoc, T.; Nguyen Trong, D.; Talu, S. Effect of doped H, Br, Cu, Kr, Ge, As and Fe on structural features and bandgap of poly $C_{13}H_8$OS-X: a DFT calculation. *Des. Monomers Polym.* **2021**, *24*, 53−62.
(24) Kokilaramani, S.; Al-Ansari, M. M.; Rajasekar, A.; Al-Khattaf, F. S.; Hussain, A.; Govarthanan, M. Microbial influenced corrosion of processing industry by re-circulating waste water and its control measures. *Chemosphere* **2021**, *265*, 129075.
(25) Muthukumar, N.; Rajasekar, A.; Ponmariappan, S.; Mohanan, S.; Maruthamuthu, S.; Muralidharan, S.; Subramanian, P.; Palaniswamy, N.; Raghavan, M. Microbiologically influenced corrosion in petroleum product pipelines-a review. *Indian J. Exp. Biol.* **2003**, *41*, 1012.
(26) Punniyakotti, P.; Punniyakotti, E.; Obuli, P. K.; Yen, P. T.; Aruliah, R. A review on biodegradation of hydrocarbon and their influence on corrosion of carbon steel with special reference to petroleum industry. *J. Environ. Biotechnol. Res.* **2017**, *6*, 12−33.
(27) Kokilaramani, S.; Rajasekar, A.; AlSalhi, M. S.; Devanesan, S. Characterization of methanolic extract of seaweeds as environmentally benign corrosion inhibitors for mild steel corrosion in sodium chloride environment. *J. Mol. Liq.* **2021**, *340*, 117011.
(28) Švorc, Ĺ. Determination of caffeine: a comprehensive review on electrochemical methods. *Int. J. Electrochem. Sci.* **2013**, *8*, 5755−5773.
(29) Kumar, G. G.; Gowtham, S. M. Recent advancements, key challenges and solutions in non-enzymatic electrochemical glucose sensors based on graphene platforms. *RSC Adv.* **2017**, *7*, 36949−36976.
(30) Xie, T.; et al. A facile molecularly imprinted electrochemical sensor based on graphene: application to the selective determination of thiamethoxam in grain. *RSC Adv.* **2017**, *7*, 38884.
(31) Švorc, L. u.; Tomčík, P.; Svítková, J.; Rievaj, M.; Bustin, D. Voltammetric determination of caffeine in beverage samples on bare boron-doped diamond electrode. *Food Chem.* **2012**, *135*, 1198−1204.
(32) Redivo, L.; Stredanský, M.; De Angelis, E.; Navarini, L.; Resmini, M.; Švorc, Ĺ. Bare carbon electrodes as simple and efficient sensors for the quantification of caffeine in commercial beverages. *R. Soc. Open Sci.* **2018**, *5*, 172146.
(33) Tyszczuk-Rotko, K.; Bęczkowska, I. Nafion covered lead film electrode for the voltammetric determination of caffeine in beverage samples and pharmaceutical formulations. *Food Chem.* **2015**, *172*, 24−29.
(34) Yiğit, A.; Yardım, Y.; Çelebi, M.; Levent, A.; Şentürk, Z. Graphene/Nafion composite film modified glassy carbon electrode for simultaneous determination of paracetamol, aspirin and caffeine in pharmaceutical formulations. *Talanta* **2016**, *158*, 21−29.
(35) Sadok, I.; Tyszczuk-Rotko, K.; Nosal-Wiercińska, A. Bismuth particles Nafion covered boron-doped diamond electrode for simultaneous and individual voltammetric assays of paracetamol and caffeine. *Sens. Actuators, B* **2016**, *235*, 263−272.
(36) Yang, Z. N.; Zhang, Z.; Zhang, J. Q. Electrodeposition of decorative and protective Zn-Fe coating onto low-carbon steel substrate. *Surf. Coating. Technol.* **2006**, *200*, 4810−4815.
(37) Srikarun, B.; Prapas, M. The effect of iron-based hardfacing with chromium powder addition onto low carbon steel. *Mater. Today: Proc.* **2018**, *5*, 9272−9280.
(38) Lecante, A.; Robert, F.; Blandinières, P. A.; Roos, C. Anti-corrosive properties of S. tinctoria and G. ouregou alkaloid extracts on low carbon steel. *Curr. Appl. Phys.* **2011**, *11*, 714−724.
(39) Shirakawa, H.; McDiarmid, A.; Heeger, A. Twenty-five years of conducting polymer. *Chem. Commun.* **2003**, 1−4.
(40) Ryu, H.; Sheng, N.; Ohtsuka, T.; Fujita, S.; Kajiyama, H. Polypyrrole film on 55% Al−Zn-coated steel for corrosion prevention. *Corros. Sci.* **2012**, *56*, 67−77.
(41) Fenelon, A. M.; Breslin, C. B. The electropolymerization of pyrrole at a CuNi electrode: corrosion protection properties. *Corros. Sci.* **2003**, *45*, 2837−2850.
(42) El Jaouhari, A.; El Asbahani, A.; Bouabdallaoui, M.; Aouzal, Z.; Filotás, D.; Bazzaoui, E. A.; Nagy, G.; Bazzaoui, M.; Albourine, A.; Hartmann, D. Corrosion resistance and antibacterial activity of electrosynthesized polypyrrole. *Synth. Met.* **2017**, *226*, 15−24.
(43) Lei, Y.; Sheng, N.; Hyono, A.; Ueda, M.; Ohtsuka, T. Electrochemical synthesis of polypyrrole films on copper from phytic solution for corrosion protection. *Corros. Sci.* **2013**, *76*, 302−309.
(44) Grubač, Z.; Rončević, I. Š.; Metikoš-Huković, M. Corrosion properties of the Mg alloy coated with polypyrrole films. *Corros. Sci.* **2016**, *102*, 310−316.
(45) Rammelt, U.; Duc, L. M.; Plieth, W. Improvement of protection performance of polypyrrole by dopant anions. *J. Appl. Electrochem.* **2005**, *35*, 1225−1230.
(46) Flamini, D. O.; Saugo, M.; Saidman, S. B. Electrodeposition of polypyrrole on Nitinol alloy in the presence of inhibitor ions for corrosion protection. *Corros. Sci.* **2014**, *81*, 36−44.
(47) Qi, K.; Qiu, Y.; Chen, Z.; Guo, X. Corrosion of conductive polypyrrole: Galvanic interactions between polypyrrole and metal substrates. *Corros. Sci.* **2015**, *91*, 272−280.
(48) Umoren, S. A.; Solomon, M. M. Protective polymeric films for industrial substrates: A critical review on past and recent applications with conducting polymers and polymer composites/nanocomposites. *Prog. Mater. Sci.* **2019**, *104*, 380−450.

https://doi.org/10.1021/acsomega.2c01561
ACS Omega 2022, 7, 19842−19852

(49) Plieth, W.; Bund, A.; Rammelt, U.; Neudeck, S.; Duc, L. The role of ion and solvent transport during the redox process of conducting polymers. *Electrochim. Acta* **2006**, *51*, 2366−2372.
(50) Uebel, M.; Exbrayat, L.; Rabe, M.; Tran, T. H.; Crespy, D.; Rohwerder, M. On the Role of Trigger Signal Spreading Velocity for Efficient Self-Healing Coatings for Corrosion Protection. *J. Electrochem. Soc.* **2018**, *165*, C1017−C1027.
(51) Huang, L.; Li, J.; Yuan, W.; Liu, X.; Li, Z.; Zheng, Y.; Liang, Y.; Zhu, S.; Cui, Z.; Yang, X.; Yeung, K. W. K.; Wu, S. Near-infrared light controlled fast self-healing protective coating on magnesium alloy. *Corros. Sci.* **2020**, *163*, 108257.
(52) Paliwoda-Porebska, G.; Stratmann, M.; Rohwerder, M.; Potje-Kamloth, K.; Lu, Y.; Pich, A. Z.; Adler, H.-J. On the development of polypyrrole coatings with self-healing properties for iron corrosion protection. *Corros. Sci.* **2005**, *47*, 3216−3233.
(53) Stankiewicz, A.; Szczygieł, I.; Szczygieł, B. Self-healing coatings in anti-corrosion applications. *J. Mater. Sci.* **2013**, *48*, 8041−8051.
(54) Hien, N. T. L.; Garcia, B.; Pailleret, A.; Deslouis, C. Role of doping ions in the corrosion protection of iron by polypyrrole films. *Electrochim. Acta* **2005**, *50*, 1747−1755.
(55) Mrad, M.; Dhouibi, L.; Montemor, M. F.; Triki, E. Effect of doping by corrosion inhibitors on the morphological properties and the performance against corrosion of polypyrrole electrodeposited on AA6061-T6. *Prog. Org. Coat.* **2011**, *72*, 511−516.
(56) Karpakam, V.; Kamaraj, K.; Sathiyanarayanan, S.; Venkatachari, G.; Ramu, S. Electrosynthesis of polyaniline−molybdate coating on steel and its corrosion protection performance. *Electrochim. Acta* **2011**, *56*, 2165−2173.
(57) Lenz, D. M.; Delamar, M.; Ferreira, C. A. Improvement of the anticorrosion properties of polypyrrole by zinc phosphate pigment incorporation. *Prog. Org. Coat.* **2007**, *58*, 64−69.
(58) Adhikari, A.; Claesson, P.; Pan, J.; Leygraf, C.; Dédinaité, A.; Blomberg, E. Electrochemical behavior and anticorrosion properties of modified polyaniline dispersed in polyvinylacetate coating on carbon steel. *Electrochim. Acta* **2008**, *53*, 4239−4247.
(59) Jensen, M. B.; Peterson, M. J.; Jadhav, N.; Gelling, V. J. SECM investigation of corrosion inhibition by tungstate- and vanadate-doped polypyrrole/aluminum flake composite coatings on AA2024-T3. *Prog. Org. Coat.* **2014**, *77*, 2116−2122.
(60) Solmaz, R.; Kardaş, G. Electrochemical synthesis and characterization of poly-2-aminothiazole. *Prog. Org. Coat.* **2009**, *64*, 81−88.
(61) Keleş, H.; Solmaz, R.; Özcan, M.; Kardaş, G.; Dehri, İ. Copper modified poly-6-amino-m-cresol (poly-AmC/Cu) coating for mild steel protection. *Surf. Coat. Technol.* **2009**, *203*, 1469−1473.
(62) Xu, J.; Zhang, Y.; Zhang, D.; Tang, Y.; Cang, H. Electrosynthesis of PAni/PPy coatings doped by phosphotungstate on mild steel and their corrosion resistance. *Prog. Org. Coat.* **2015**, *88*, 84−91.
(63) Jadhav, N.; Matsuda, T.; Gelling, V. Mica/polypyrrole (doped) composite containing coatings for the corrosion protection of cold-rolled stee. *J. Coating Technol. Res.* **2018**, *15*, 363−374.
(64) Liu, A. S.; da Silva, E. M. F.; Cho, L. Y. The Chemical Deposition of Polypyrrole at a Copper Surface Varying Concentrations of Salicylic Acid in the Reactive Medium. *Mater. Sci. Forum* **2020**, *1012*, 447−452.
(65) Annibaldi, V.; Rooney, A. D.; Breslin, C. B. Corrosion protection of copper using polypyrrole electrosynthesised from a salicylate solution. *Corros. Sci.* **2012**, *59*, 179−185.
(66) González, M. B.; Saidman, S. B. Corrosion protection properties of polypyrrole electropolymerized onto steel in the presence of salicylate. *Prog. Org. Coat.* **2012**, *75*, 178−183.
(67) Hung, H. M.; Linh, D. K.; Chinh, N. T.; Duc, L. M.; Trung, V. Q. Improvement of the corrosion protection of polypyrrole coating for CT3 mild steel with 10-camphor sulfonic acid and molybdate as inhibitor dopants. *Prog. Org. Coat.* **2019**, *131*, 407−416.
(68) Quoc Trung, V.; Hong Hanh, T.; Hong Quang, T.; Manh Hung, H.; Khanh Linh, D.; Thi Tuyet Lan, H.; Minh Duc, L. Corrosion protection of molybdate doped polypyrrole film prepared in succinic acid solution. *Corrosion Eng. Sci. Technol.* **2018**, *53*, 59−66.
(69) Trung, V. Q.; Van Hoan, P.; Phung, D. Q.; Duc, L. M.; Hang, L. T. T. Double corrosion protection mechanism of molybdate-doped polypyrrole/montmorillonite nanocomposites. *J. Exp. Nanosci.* **2014**, *9*, 282−292.
(70) Beck, F.; Michaelis, R.; Schloten, F.; Zinger, B. Filmforming electropolymerization of pyrrole on iron in aqueous oxalic acid. *Electrochim. Acta* **1994**, *39*, 229−234.
(71) Chen, Z.; Yang, W.; Xu, B.; Guo, Y.; Chen, Y.; Yin, X.; Liu, Y. Corrosion behaviors and physical properties of polypyrrole-molybdate coating electropolymerized on carbon steel. *Prog. Org. Coat.* **2018**, *122*, 159−169.
(72) Kasisomayajula, S. V.; Qi, X.; Vetter, C.; Croes, K.; Pavlacky, D.; Gelling, V. J. A structural and morphological comparative study between chemically synthesized and photopolymerized poly(pyrrole). *J. Coat. Technol. Res.* **2010**, *7*, 145−158.
(73) Cysewska, K.; Gazda, M.; Jasiński, P. Influence of electropolymerization temperature on corrosion, morphological and electrical properties of PPy doped with salicylate on iron. *Surf. Coat. Technol.* **2017**, *328*, 248−255.

https://doi.org/10.1021/acsomega.2c01561
ACS Omega 2022, 7, 19842−19852